Optics Letters

Multi-focus hologram utilizing Pancharatnam–Berry phase elements based metamirror

Yue Wang,[1,†] Chunsheng Guan,[1,†] Xumin Ding,[1,*] Kuang Zhang,[1,3] Badreddine Ratni,[2] Shah Nawaz Burokur,[2,4] Xuemai Gu,[1] and Qun Wu[1]

[1]Harbin Institute of Technology, Department of Microwave Engineering, Harbin 150001, China
[2]LEME, UPL, Univ Paris Nanterre, F92410 Ville d'Avray, France
[3]e-mail: zhangkuang@hit.edu.cn
[4]e-mail: sburokur@parisnanterre.fr
*Corresponding author: xuminding@hit.edu.cn

Received 25 January 2019; revised 24 March 2019; accepted 27 March 2019; posted 27 March 2019 (Doc. ID 358706); published 19 April 2019

An ultrathin reflection-type metamirror is proposed for multi-focusing with any desired focusing fashion including focal number and location. The metamirror is composed of reflection-type Pancharatnam–Berry (P-B) phase elements, which are able to provide full reflection phase of 2π, together with near-unity reflection efficiency by judiciously engineering the rotation angle of each latter element. A holographic algorithm is utilized to calculate the phase distribution at the interface of the metamirror to achieve the desired multi-focus spots. Experimental demonstrations performed in microwave region show good imaging quality with high reflection efficiency and imaging efficiency. The proposed metamirror provides a high-performance solution for low-cost and lightweight beam-shaping and beam-focusing devices.

https://doi.org/10.1364/OL.44.002189

Metasurface, a new subcategory of metamaterial, has attracted much attention due to its outstanding ability in manipulating wavefronts by introducing abrupt phase discontinuities at the interface. Compared to 3D multilayer metamaterial, metasurface offers the benefits of negligible thickness, reduced absorption losses, and low cost of fabrication. Generally, a metasurface is constituted by a two-dimensional (2D) array of subwavelength resonators with specifically designed geometry [1] and orientation [2,3] to manipulate the local phase and amplitude of a scattering wave. So far, phase discontinuities-based metasurfaces have been implemented for various optical functionalities, such as optical vortices [4–6], beam deflection and focusing [7,8], hologram imaging [9–15], and beam-shaping [16,17], showing great potentials in wave front manipulation. Pancharatnam–Berry (P-B) phase elements based metasurface is a planar artificial structure with specific rotational orientation and angle under circularly-polarized (CP) incidence [18–20].

One of the most striking applications of metasurfaces is metalens or metamirror for miniaturization and multifunction applications, holding promises for system integration. For metalens operating in transmission mode, the performance is closely related to the transmission efficiency, which usually remains to a fairly low value due to the fundamental limits and intrinsic Ohmic losses. The maximum efficiency achieved with single-layer ultrathin metasurface has been shown to be of the order of only a few percent [1,2,17]. Different transmission-type metasurfaces, for example, dielectric metasurfaces [21], Huygens' metasurfaces [22], multilayered metascreens, and meta-transmitarrays [23,24] have been proposed to improve the efficiency. However, these designs require a finite minimum thickness, together with significant fabrication challenges and frequency dispersion. Metamirror [25,26], a reflection-type metasurface composed of artificial meta-atoms printed on a thin dielectric substrate backed by a metal ground plane, is not only able to operate over a broad wavelength range but also keeps a high manipulation efficiency. Therefore, metamirrors have been validated as efficient reflectors [27], wave plates [28–31], blazed gratings [16], and holograms [32–34].

Recently, we proposed a theoretical approach based on spatial energy distribution manipulation to achieve multi-focus pattern in one-dimensional (1D) space from a Huygens' metamirror [35], where the phase distribution is applied along only one axis. In this Letter, we experimentally demonstrate the convergence of a circularly-polarized incident wave to any desired position using a reflection-type P-B phase elements based metamirror with a relatively high efficiency. Based on the proposed P-B phase elements, a multi-focus metamirror for converging the incident beam to specific positions is validated in both simulations and measurements. Here a holographic algorithm is utilized to calculate the phase distribution across the metasurface. The simulated results of four-focus and five-focus metamirrors show good qualitative agreements with theoretical calculations, implying that the proposed holography based metamirror can achieve arbitrary focusing point number and location. To further validate the performance of the proposed metamirror, a four-focus metamirror is fabricated and measured. The experimental result agrees qualitatively with theoretical and numerical simulation results, indicating the high efficiency performance and feasibility of the proposed metamirror.

The building blocks used to construct the multi-focus metamirror are a set of reflection-type P-B phase elements, as shown in Fig. 1(b). Each elementary element is composed of a double-split ring resonator (DSRR) placed on the metal ground with a thin dielectric substrate in between. According to the P-B phase principle [22,36], an abrupt phase change, which is twice of the rotation angle of the unit cells, can be introduced to the cross-polarized component defined as the electromagnetic wave having its electric field rotated in an opposite direction with regard to the incident wave. Thus, by appropriately designing the rotation angle, any desired reflection phase can be introduced to the cross-polarized component. The proposed unit cell is simulated using the commercial software CST Microwave Studio by applying unit cell boundary conditions in x- and y-directions under right-hand circularly polarized (RHCP) incidence, and the simulated results at 10 GHz are shown in Fig. 1(a). The phase change can cover the whole range of 2π, while the amplitude of the reflection coefficient keeps near unity, indicating that almost all the incident energy can be transformed to the cross-polarized component, which is the left-hand circularly polarized (LHCP) wave, by the proposed unit cells. The near-unity reflection also enables super conversion efficiency compared to the maximum conversion efficiency of 25% in previous single-layer thin metasurface design [3]. Here, we stress on the fact that the thickness of the proposed unit cell structure is only 2 mm ($\lambda_0/15$ at the operating frequency of 10 GHz), and there is no need to change the shape or the geometrical dimensions of the unit cell, which greatly simplifies the design process.

In order to achieve the desired multi-focus pattern, phase distribution across the metasurface is calculated by the proposed holographic algorithm. The method to realize multi-focus pattern consists in selecting ideal point sources as virtual sources at the positions of the pre-designed focal positions, as illustrated in Fig. 2 [35,37]. By superposing radiated field generated by all virtual sources, which can be described by Green function, the virtual electric field distribution can be obtained. Then the virtual electric field can be mapped onto the recording plane where the metamirror is located and the phase delay $\varphi(x_j, y_j, 0)$ ($j = 1$ to M) for each meta-atom at the position of $(x_j, y_j, 0)$ can be calculated. Since the calculation of phase

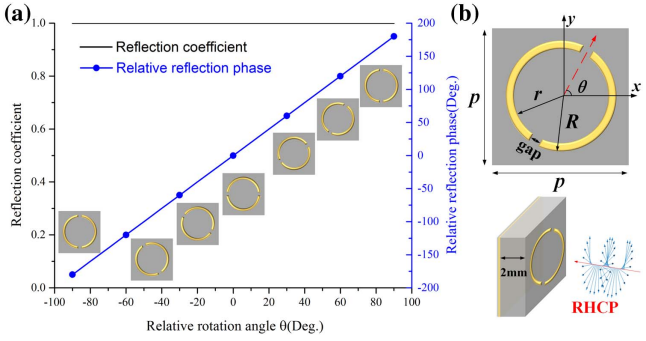

Fig. 1. Numerical characterization results of reflection-type P-B phase elements. (a) P-B geometric phase variation (blue line) and reflection coefficient (black line) of cross-polarized reflected wave. (b) Schematic of unit cell composed of copper double-split ring resonator (DSRR) ($r = 2.4$ mm, $R = 2.6$ mm, gap $= 0.5$ mm, $p = 6$ mm) printed on a copper-backed dielectric substrate having relative permittivity $\varepsilon_r = 3.5$ and thickness of 2 mm.

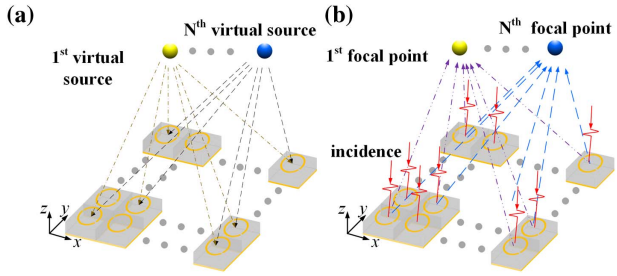

Fig. 2. Schematic principle of the proposed holographic imaging process. (a) Virtual and (b) reconstructed electric field for multi-focus metamirror.

conjugation is equivalent to the time reversal for the incident monochromatic wave, the phase delay of each meta-atom should be set as $-\varphi(x_j, y_j, 0)$ to achieve the desired focusing imaging. In order to keep uniform focal intensity of focal points, the weight factor w_i is introduced to modify the phase distribution on the metamirror. An iterative procedure is proposed to obtain the modified phase distribution $-\varphi(x_j, y_j, 0)$ ($j = 1$ to M), as follows:

$$-\phi_j^p = -\arg\left(\sum_{i=1}^{N} \frac{w_i^p E_i^{p-1}}{|E_i^{p-1}|} \frac{e^{-jkr_{ji}}}{r_{ji}}\right), \tag{1}$$

where $r_{ji} = \sqrt{(x_j - x_i)^2 + (y_j - y_i)^2 + (z_i)^2}$ is the distance between jth meta-atom located at $(x_j, y_j, 0)$ ($j = 1$ to M) and ith focal point at (x_i, y_i, z_i) ($i = 1$ to N), k is the phase constant, and the superscript p represents the pth iterative step. $|E_i^{p-1}|$ denotes the electric field intensity of the ith focal point in the $(p-1)$th iterative step.

As the phase delay of each meta-atom located at $(x_j, y_j, 0)$ is determined to be $-\varphi(x_j, y_j, 0)$, the reconstructed field can be calculated by superposing the field component emitted by each meta-atom. Since the radiation of the meta-atom also obeys the Greens' function, the reconstructed electric field at the position of each focal point can be retrieved as

$$E_i^p = \sum_{j=1}^{M} \frac{e^{-ikr_{ji} + i\varphi_j^p}}{r_{ji}}, \tag{2}$$

$$w_i^p = w_i^{p-1} \frac{\sum_{i=1}^{N} |E_i^{p-1}|}{N|E_i^{p-1}|}. \tag{3}$$

To demonstrate our proposed theory, four-focus and five-focus metamirrors with uniform focal intensity distribution are designed. In the near field imaging simulations, metamirrors are characterized with open boundary conditions along x- and y-axes and illuminated by a normally incident RHCP wave at 10 GHz. For consideration of high resolution, the imaging (xoy) plane is designed to be 3.33λ and 5λ away from the metamirror, respectively, for the four-focus and five-focus hologram. According to the definition of the far-field region $r \approx 2D^2/\lambda$, where D is the diagonal dimension of the metamirrors. The considered focal distances 3.3λ and 5λ are located within the near-field region. The electric field intensity distribution in both xoy and xoz planes for the two cases are shown in Fig. 3. Figures 3(a) and 3(d) show the theoretical calculation

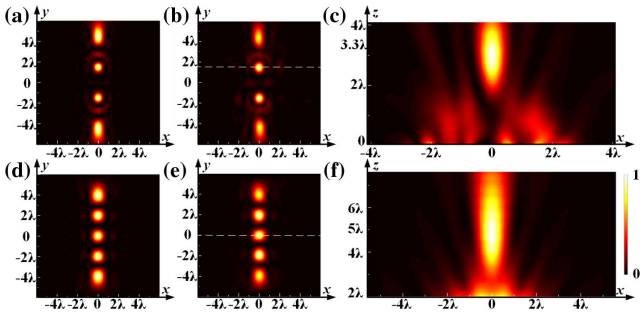

Fig. 3. Results of the centered multi-focus metamirrors. (a) and (d) Theoretical result, (b) and (e) simulated result in imaging (xoy) plane, (c) and (f) simulated result in the $y = 1.5\lambda$ and $y = 0$ planes, respectively.

results, and Figs. 3(b) and 3(e) present the simulated results in the imaging plane. Figures 3(c) and 3(f) depict the simulated results in the $y = 1.5\lambda$ and $y = 0$ planes for the four-focus and five-focus hologram, respectively. The positions of the focus points for the four-focus metamirror along y-axis are designed to be -4.5λ, -1.5λ, 1.5λ, and 4.5λ, and the simulated focus points are found to be -4.4λ, -1.5λ, 1.5λ, and 4.4λ. In the same manner, the positions of the focus points for the five-focus metamirror are designed to be -4λ, -2λ, 0, 2λ, and 4λ along y-axis, and simulation results show focusing at -3.9λ, -1.93λ, 0, 1.93λ, and 3.9λ. It can be clearly observed from the simulation results that the incident wave is successfully converged to the pre-designed focal points. The conversion efficiency is simulated to be 81.59% and 81.34%, respectively, for the four-focus and five-focus metamirrors.

Moreover, multi-focus pattern deviating from the central line of the imaging plane are designed from the proposed high efficiency arbitrary focal positions metamirrors. Focal points are designed to be located along the line of $x = 2.6\lambda$ for the four-focus metamirror and $x = 4\lambda$ for the five-focus metamirror. Figures 4(a) and 4(d) show the theoretical calculations, and Figs. 4(b) and 4(e) present the simulated results. Figures 4(c) and 4(f) depict the phase distribution at the interface of the two metamirrors calculated by the proposed holographic algorithm. For both metamirrors, the numerical simulations show good agreement with the theoretical designs.

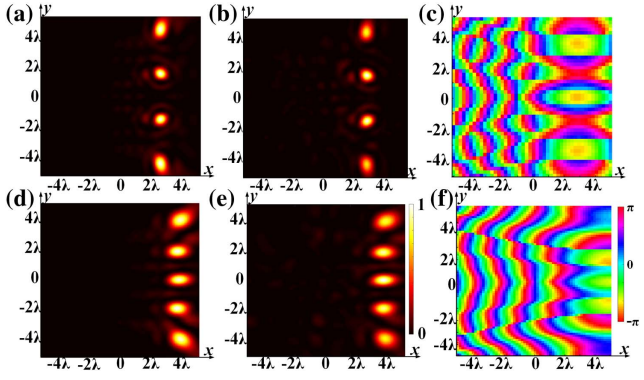

Fig. 4. Results of the off-centered multi-focus metamirrors. Theoretical and simulated results of the electric field intensity distribution and phase distribution: (a)–(c) four-focus metamirror and (d)–(f) five-focus metamirror.

To further verify the performances of the proposed metamirror, the off-centered four-focus metamirror with $46 * 46$ meta-atoms is fabricated using conventional printed circuit board (PCB) technique. Measurements are performed using a near-field scanning system with a fiber-optic active antenna fixed on two orthogonal translation stages controlled by a motion controller and connected to one port of the vector network analyzer (VNA). A feeding RHCP horn antenna connected to the other port of the VNA is placed about 20λ away from the metamirror to guarantee a quasi-plane wave illumination at 10 GHz. Since measuring transmission coefficient in the imaging plane of the metamirror involves collecting both incident and reflected electric fields, another measurement without the metamirror is performed to collect only the incident electric field as reference. The reference data is then subtracted from the first measurement (with metamirror) to obtain only the reflected electric field. Electric field polarized along x- and y-axes is measured respectively, and the LHCP and RHCP components can be calculated as $E_{\mathrm{LHCP}} = \frac{1}{\sqrt{2}}(E_x - iE_y)$ and $E_{\mathrm{RHCP}} = \frac{1}{\sqrt{2}}(E_x + iE_y)$. Figure 5(a) presents the measured electric field intensity distribution at 10 GHz and Fig. 5(b) shows the normalized intensity profiles along $x = 2.6\lambda$. The measured positions of the focal points are located at (2.73λ, -4.53λ), (2.67λ, -1.4λ), (2.6λ, 2.07λ), and (2.93λ, 5.07λ). The first and second focal points deviate only slightly away from their respective predesigned positions of (2.6λ, -4.5λ) and (2.6λ, -1.5λ), and the corresponding measured intensity distribution of the first focal point is weaker. The third focal point deviates only along the y-axis by 0.57λ. However, the fourth focal point presents a higher deviation along both x- and y-axes. The main reason for this discrepancy is presumably related to the feeding horn antenna deviating slightly off the central axis of the metamirror, causing consequent deviation of the fourth focal point.

Three parameters are adopted here to evaluate the imaging quality of the holographic metamirror [37]: imaging efficiency, signal-to-noise ratio (SNR), and root-mean-square error (RMSE). The imaging efficiency, describing the ability to transform the incident energy to the preset focal points, is calculated by the energy concentrated in the preset focal points referenced to the total energy on the measured plane. The SNR is used to describe the ratio between the peak intensity in the image to the standard deviation of the background noise, which can be calculated by

$$\mathrm{SNR} = 10\ \lg(P_s/P_n), \tag{4}$$

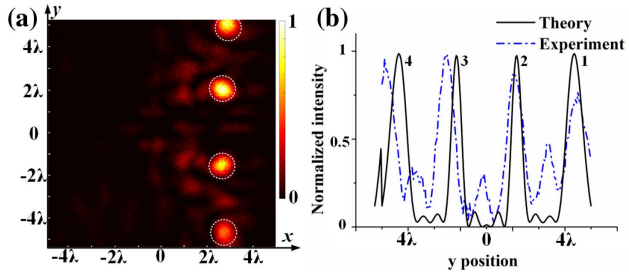

Fig. 5. Experimental results for the off-centered four-focus metamirror. (a) Electric field intensity distribution. (b) Normalized intensity profiles along $x = 2.6\lambda$.

where P_s is the peak intensity in the reconstructed image and P_n is the standard deviation of the background noise. The RMSE, defined as the deviations between the measured intensity ratios and theoretical values, is used to evaluate the manipulation ability of energy allocation of focal points. It can be calculated as

$$\sigma = \sqrt{\frac{1}{N}\sum_{n=1}^{N}\left(\frac{|E_n|}{\sum_{n=1}^{N}|E_n|} - \frac{s_n}{\sum_{n=1}^{N}s_n}\right)^2}. \quad (5)$$

The parameters to evaluate the manipulation ability are calculated from the experimental data. The radius of each focal point is set to be $\lambda/2$, and the imaging efficiency reaches a high level of 57.8%, indicating that more than half of the energy on the measured plane is concentrated on the focal points. RMSE of the off-centered four-focus metamirror is calculated to be 5.17%, indicating little deviation between theoretical design and measurement when the incident energy is transformed to the pre-designed focal points equally. The SNR is calculated to be as high as 13.2. Consequently, the experimental results validate the high efficiency and good imaging quality of our proposed multi-focus metamirror.

In conclusion, high efficiency multi-focus metamirrors based on reflection-type P-B phase elements are designed and validated. The simulated and measured images of multi-focus metamirrors show good qualitative agreement with the theoretical analysis, and the experimental measurement performed on an off-centered four-focus metamirror achieves high quality with an imaging efficiency of 57.8%, SNR of 13.22 and RMSE of only 5.17%. The proposed concept of metamirror holograms expands the route to microwave applications on holographic technologies, including computer-generated holograms, antennas, illusions, security, and data storage.

Funding. National Natural Science Foundation of China (NSFC) (61701141); China Postdoctoral Science Foundation (2016M600248, 2018T110298).

†These authors contributed equally to this Letter.

REFERENCES

1. N. Yu, P. Genevet, M. A. Kats, F. Aieta, J. P. Tetienne, F. Capasso, and Z. Gaburro, Science **334**, 333 (2011).
2. E. Hasman, V. Kleiner, G. Biener, and A. Niv, Appl. Phys. Lett. **82**, 328 (2003).
3. X. Ding, F. Monticone, K. Zhang, L. Zhang, D. Gao, S. N. Burokur, A. de Lustrac, Q. Wu, C. W. Qiu, and A. Alù, Adv. Mater. **27**, 1195 (2015).
4. Y. Lai, J. Ng, H. Chen, D. Han, J. Xiao, Z.-Q. Zhang, and C. T. Chan, Phys. Rev. Lett. **102**, 253902 (2009).
5. K. Zhang, Y. Yuan, D. Zhang, X. Ding, B. Ratni, S. N. Burokur, M. Lu, K. Tang, and Q. Wu, Opt. Express **26**, 1351 (2018).
6. Y. Yuan, K. Zhang, X. Ding, B. Ratni, S. N. Burokur, and Q. Wu, Photon. Res. **7**, 80 (2019).
7. J. B. Pendry, Phys. Rev. Lett. **85**, 3966 (2000).
8. N. Fang, H. Lee, C. Sun, and X. Zhang, Science **308**, 534 (2005).
9. S. A. Kuznetsov, M. A. Astafev, M. Beruete, and M. Navarro-Cía, Sci. Rep. **5**, 7738 (2015).
10. G. S. Lipworth, J. A. Hagerty, D. Arnitz, Y. A. Urzhumov, D. R. Nash, R. J. Hannigan, C. T. Tegreene, and M. S. Reynolds, in *IEEE/MTT-S International Microwave Symposium (IMS)* (IEEE, 2018), pp. 964–967.
11. N. W. Caira and D. R. Smith, Appl. Opt. **57**, A19 (2018).
12. G. Lipworth, N. W. Caira, S. Larouche, and D. R. Smith, Opt. Express **24**, 19372 (2016).
13. C. M. Watts, D. Shrekenhamer, J. Montoya, G. Lipworth, J. Hunt, T. Sleasman, S. Krishna, D. R. Smith, and W. J. Padilla, Nat. Photonics **8**, 605 (2014).
14. W. Wan, J. Gao, and X. Yang, Adv. Opt. Mater. **5**, 1700541 (2017).
15. S. Choudhury, U. Guler, A. Shaltout, V. M. Shalaev, A. V. Kildishev, and A. Boltasseva, Adv. Opt. Mater. **5**, 1700196 (2017).
16. S. Sun, K. Y. Yang, C. M. Wang, T. K. Juan, W. T. Chen, C. Y. Liao, Q. He, S. Xiao, W. T. Kung, and G. Y. Guo, Nano Lett. **12**, 6223 (2012).
17. X. Ni, N. K. Emani, A. V. Kildishev, A. Boltasseva, and V. M. Shalaev, Science **335**, 427 (2012).
18. P. Chen, L. L. Ma, W. Duan, J. Chen, S. J. Ge, Z. H. Zhu, M. J. Tang, R. Xu, W. Gao, T. Li, W. Hu, and Y. Q. Lu, Adv. Mater. **30**, 1705865 (2018).
19. S. Zheng, Y. Li, Q. Lin, X. Zeng, G. Zheng, Y. Cai, Z. Chen, S. Xu, and D. Fan, Photon. Res. **6**, 385 (2018).
20. H. Larocque, J. Gagnon-Bischoff, D. Mortimer, Y. Zhang, F. Bouchard, J. Upham, V. Grillo, R. W. Boyd, and E. Karimi, Opt. Express **25**, 19832 (2017).
21. D. Lin, P. Fan, E. Hasman, and M. L. Brongersma, Science **345**, 298 (2014).
22. C. Pfeiffer and A. Grbic, Phys. Rev. Lett. **110**, 197401 (2013).
23. N. K. Grady, J. E. Heyes, D. R. Chowdhury, Y. Zeng, M. T. Reiten, A. K. Azad, A. J. Taylor, D. A. Dalvit, and H. T. Chen, Science **340**, 1304 (2013).
24. F. Monticone, N. M. Estakhri, and A. Alù, Phys. Rev. Lett. **110**, 203903 (2013).
25. X. Li, S. Xiao, B. Cai, Q. He, T. J. Cui, and L. Zhou, Opt. Lett. **37**, 4940 (2012).
26. A. Pors, M. G. Nielsen, R. L. Eriksen, and S. I. Bozhevolnyi, Nano Lett. **13**, 829 (2013).
27. B. Ratni, A. de Lustrac, G.-P. Piau, and S. N. Burokur, Opt. Express **26**, 2613 (2018).
28. J. Hao, Q. Ren, Z. An, X. Huang, Z. Chen, M. Qiu, and L. Zhou, Phys. Rev. A **80**, 023807 (2009).
29. A. Pors and S. I. Bozhevolnyi, Opt. Express **21**, 2942 (2013).
30. B. Ratni, A. de Lustrac, G.-P. Piau, and S. N. Burokur, Appl. Phys. Lett. **111**, 214101 (2017).
31. A. Pors, M. G. Nielsen, and S. I. Bozhevolnyi, Opt. Lett. **38**, 513 (2013).
32. G. Zheng, H. Mühlenbernd, M. Kenney, G. Li, T. Zentgraf, and S. Zhang, Nat. Nanotechnol. **10**, 308 (2015).
33. W. T. Chen, K. Y. Yang, C. M. Wang, Y. W. Huang, G. Sun, I. D. Chiang, C. Y. Liao, W. L. Hsu, H. T. Lin, and S. Sun, Nano Lett. **14**, 225 (2013).
34. L. Li, T. J. Cui, W. Ji, S. Liu, J. Ding, X. Wan, Y. B. Li, M. Jiang, C. W. Qiu, and S. Zhang, Nat. Commun. **8**, 197 (2017).
35. Z. Wang, X. Ding, K. Zhang, and Q. Wu, Sci. Rep. **7**, 9081 (2017).
36. Z. E. Bomzon, G. Biener, V. Kleiner, and E. Hasman, Opt. Lett. **27**, 1141 (2002).
37. Z. Wang, X. Ding, K. Zhang, B. Ratni, S. N. Burokur, X. Gu, and Q. Wu, Adv. Opt. Mater. **6**, 1800121 (2018).